The Astrophysical Journal Letters, 868:L14 (5pp), 2018 November 20 https://doi.org/10.3847/2041-8213/aaee82

Generation of Inverted Heliospheric Magnetic Flux by Coronal Loop Opening and Slow Solar Wind Release

Mathew J. Owens, Mike Lockwood, Luke A. Barnard, and Allan R. MacNeil
Department of Meteorology, University of Reading, Earley Gate, P.O. Box 243, Reading RG6 6BB, UK; m.j.owens@reading.ac.uk
Received 2018 September 28; revised 2018 October 29; accepted 2018 November 5; published 2018 November 19

Abstract

In situ spacecraft observations provide much-needed constraints on theories of solar wind formation and release, particularly the highly variable slow solar wind, which dominates near-Earth space. Previous studies have shown an association between local inversions in the heliospheric magnetic field (HMF) and solar wind released from the vicinity of magnetically closed coronal structures. We here show that in situ properties of inverted HMF are consistent with the same hot coronal source regions as the slow solar wind. We propose that inverted HMF is produced by solar wind speed shear, which results from interchange reconnection between a coronal loop and open flux tube, and introduces a pattern of fast–slow–fast wind along a given HMF flux tube. This same loop-opening process is thought to be central to slow solar wind formation. The upcoming *Parker Solar Probe* and *Solar Orbiter* missions provide a unique opportunity to directly observe these processes and thus determine the origin of the slow solar wind.

Key words: solar wind – Sun: activity – Sun: corona – Sun: magnetic fields

1. Introduction

A fraction of the magnetic flux that threads the photosphere reaches sufficient coronal altitude to be dragged out by the solar wind flow to form the heliospheric magnetic flux (HMF; Owens & Forsyth 2013). The integrated (unsigned) HMF is also referred to as the open solar flux (OSF). OSF can be measured in two ways. The observed photospheric magnetic field can be extrapolated up through the corona using a model and the OSF estimated as the total (unsigned) magnetic flux threading a surface at a given altitude, referred to as the source surface (Wang & Sheeley 1995). Alternatively, the HMF can be directly measured in situ, typically by spacecraft in near-Earth space, and these single-point observations assumed to be representative of the global OSF (Lockwood 2013).

While there is qualitative agreement between the two approaches, the in situ estimates are significantly larger than the photospheric magnetic field estimates. The discrepancy can be reduced by accounting for the existence of inverted HMF (Owens et al. 2017), magnetic flux that is locally folded, so that a flux tube that has a single intersection with the source surface may thread a heliocentric sphere at, e.g., 1 au, multiple times. In situ HMF observations at increasing heliocentric distance tend to result in increasingly large OSF estimates (Owens et al. 2008), suggesting inverted HMF becomes more prevalent with distance from the Sun. This is to be expected, as the increasing angle of the Parker spiral HMF to the radial direction means that smaller deviations are required to fold the HMF back toward the Sun. Such deviations can be generated by heliospheric processes—such as waves, turbulence, and draping of the HMF around fast coronal mass ejections—that twist the HMF about the nominal Parker spiral configuration. However, even accounting for inverted HMF, magnetogram-based estimates of OSF remain significantly lower than in situ estimates, suggesting the existence of open flux sources not included in the conventional picture of the steady-state coronal magnetic field (Linker et al. 2017).

While interest in inverted HMF has largely focused on OSF estimates, it may also provide insight into coronal processes. Inverted HMF has been shown to preferentially originate from dipolar- and pseudo-streamers, where open and closed coronal magnetic flux converge (Owens et al. 2013). As fast solar wind originates in relatively cool open flux regions within coronal holes and slow solar wind is associated with hotter, closed coronal loops, inverted HMF may be a result of slow wind formation and release (Fisk 2003; Antiochos et al. 2007; Crooker et al. 2012). In this Letter, we investigate the elemental composition and ion charge-state properties of inverted HMF, as these provide a diagnostic of coronal source conditions.

2. Data and Methods

Inverted HMF can be directly identified by the suprathermal electron strahl, which always moves anti-sunward, in a global sense, along the HMF (Crooker et al. 2004). In this Letter, we use inverted and uninverted HMF intervals determined by Owens et al. (2017), which combines 64 s *Advanced Composition Explorer* (*ACE*) magnetic field and suprathermal electron data (McComas et al. 1998; Smith et al. 1998) using the simple algorithm of (Owens et al. 2013). In summary, the mean 272 eV electron flux in the three pitch-angle bins centered at 90° pitch angle (i.e., perpendicular to the magnetic field direction) is used to compute the background flux. The background flux is then compared with the mean flux in the three most field-aligned pitch-angle bins (i.e., parallel to the magnetic field) and the mean flux in the three most antiparallel bins. If the parallel and/or antiparallel flux exceeds the background level by 30%, a parallel and/or antiparallel strahl is determined to exist. The radial magnetic field component is then used to determine the strahl direction in the heliospheric frame and hence the HMF topology. If the strahl is anti-sunward, the HMF is uninverted, whereas if the strahl is sunward, the HMF must be locally inverted.

HMF topology information is compared with solar wind composition and ion charge-state information provided by the *ACE* Solar Wind Ion Composition Spectrometer (SWICS) instrument (Gloeckler et al. 1998), here taken from the 1 hr "merged" data set at ftp://cdaweb.gsfc.nasa.gov/pub/data/ace/multi. The data cover 1998-01-01 to 2011-06-01. Interplanetary

coronal mass ejections (ICMEs) are removed from the steady-state solar wind, using the updated Cane & Richardson (2003) ICME catalog, available from http://www.srl.caltech.edu/ACE/ASC/DATA/level3/icmetable2.htm. It is necessary to accommodate the different time resolutions of the HMF topology and ion composition/charge-state data. The 1 hr HMF topology is taken to be the dominant (i.e., most common) 64 s HMF topology within a given hour, excluding datagaps and undetermined topologies. This gives very good agreement with the stricter requirement that a majority (i.e., at least 50%) of the 64 s topologies within a given hour be of a specific type. Over the 1998 to 2011 period with ICMEs removed, this results in 9359 hr of inverted HMF and 109,878 hr of uninverted HMF.

We compare the cumulative distribution functions (CDFs) for the inverted and uninverted HMF hours for each solar wind parameter. To quantify the effect of finite sample size, 9359 hr of uninverted HMF are randomly sampled. This is performed 1000 times and compute the 1, 2, and 3σ ranges of the resulting CDFs.

In addition to visual inspection of the CDFs, it is also useful to have a measure of the degree of difference between the inverted and uninverted distributions. We use the Kolmogorov–Smirnov (KS) non-parametric test to quantify the probability that the inverted and uninverted distributions are sub-samples of the same underlying distribution. But we also seek a measure of the magnitude of the difference in distributions (i.e., the "effect size"). The strictly standardized mean difference (SSMD) compares the difference in the mean values, μ, of two distributions in terms of their standard deviations, σ (thus it is similar to a Fischer Z-score; Zhang 2010). Assuming distributions are independent, this takes the form

$$\beta = \frac{\mu_1 - \mu_2}{\sqrt{\sigma_1^2 + \sigma_2^2}}. \quad (1)$$

As the distributions of solar wind parameters considered in this study are generally not Gaussian, we instead take a more non-parametric approach, replacing μ by the median, m, and σ by half the interquartile range (IQR), giving

$$\beta' = 2\frac{m_1 - m_2}{\sqrt{\mathrm{IQR}_1^2 + \mathrm{IQR}_2^2}}. \quad (2)$$

Here, this measure is used in a purely relative sense. However, the thresholds for low, medium, and strong effect size of 0, 0.25, and 1 (Zhang 2010) are useful guides.

3. Results

Figure 1 shows the durations of contiguous inverted and uninverted HMF intervals. An interval is defined in hourly data as lasting until a different HMF topology, an uncategorized hour or a datagap is observed. The inverted HMF intervals have a median duration of around 12 hr and an upper limit of around 3.5 days. The uninverted intervals have a median duration of around 5 days and an upper limit of around 50 days. To maximize the available data and improve statistics, we do not exclude any "buffer" region around the transition from inverted to uninverted HMF (and vice versa).

Figure 2 shows the CDFs for solar wind parameters in inverted and uninverted HMF hours. The 1, 2, and 3σ uncertainty bands resulting from limited sample size have been omitted as they are too small to be visible on the plots.

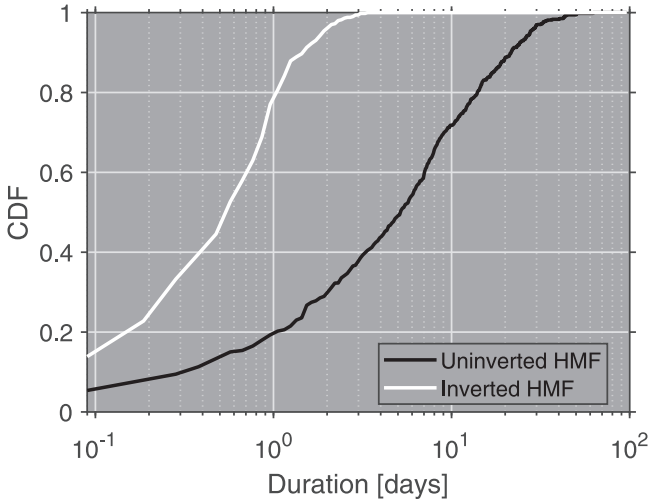

Figure 1. CDFs of the durations of contiguous uninverted (black) and inverted (white) HMF intervals in 1 hr data. Note the log scale on the *x*-axis.

Thus, for all solar wind parameters considered, the differences between inverted and uninverted HMF are not simply the result of different sample sizes. Similarly, for all solar wind parameters, the KS-test rejects the null hypothesis that the inverted and uninverted HMF distributions are sub-samples of the same underlying distribution at $p = 0.001$, i.e., the 99.9% confidence level. However, the magnitude of the differences in the inverted and uninverted distributions varies considerably for different solar wind parameters. Table 1 summarizes the β' values to quantify what can be seen by eye from the CDFs.

As reported by Owens et al. (2017), inverted HMF intervals show significantly weaker HMF intensity than uninverted HMF (panel a). Panel (b) shows inverted HMF is less radial than uninverted HMF, suggesting that (at 1 au) inverted HMF is only partially folded back on itself. Panels (c) and (d) show that inverted HMF is associated with considerably slower, and to a lesser extent, denser solar wind than uninverted HMF. There is little difference, however, between inverted and uninverted HMF in the available composition measures. While the distributions of α:p and Fe:O are statistically different, the effect is primarily in the tail of the distributions and the magnitude of the difference is very small, as indicated by the large overlap in the CDFs and the small β' values. Conversely, both the average oxygen and carbon charge states are significantly elevated in inverted HMF hours relative to uninverted HMF hours. For average iron charge states; however, the magnitude of the difference is much smaller and primarily in the tail of the distribution.

Figure 2 and Table 1 also show uninverted HMF further divided into fast and slow wind, respectively, using a simple threshold of 450 km s^{-1}. It is clear that in general, inverted HMF is much more similar to slow wind than fast wind. Indeed, inverted HMF is distinct from fast uninverted HMF in all parameters except α:p. The CDFs of Fe:O for inverted and fast uninverted HMF are clearly separated in the upper part of the distribution, despite the fairly modest β' value. Inverted HMF is nevertheless distinct from slow wind in terms of the HMF properties, which is weaker and increasingly inclined the radial direction.

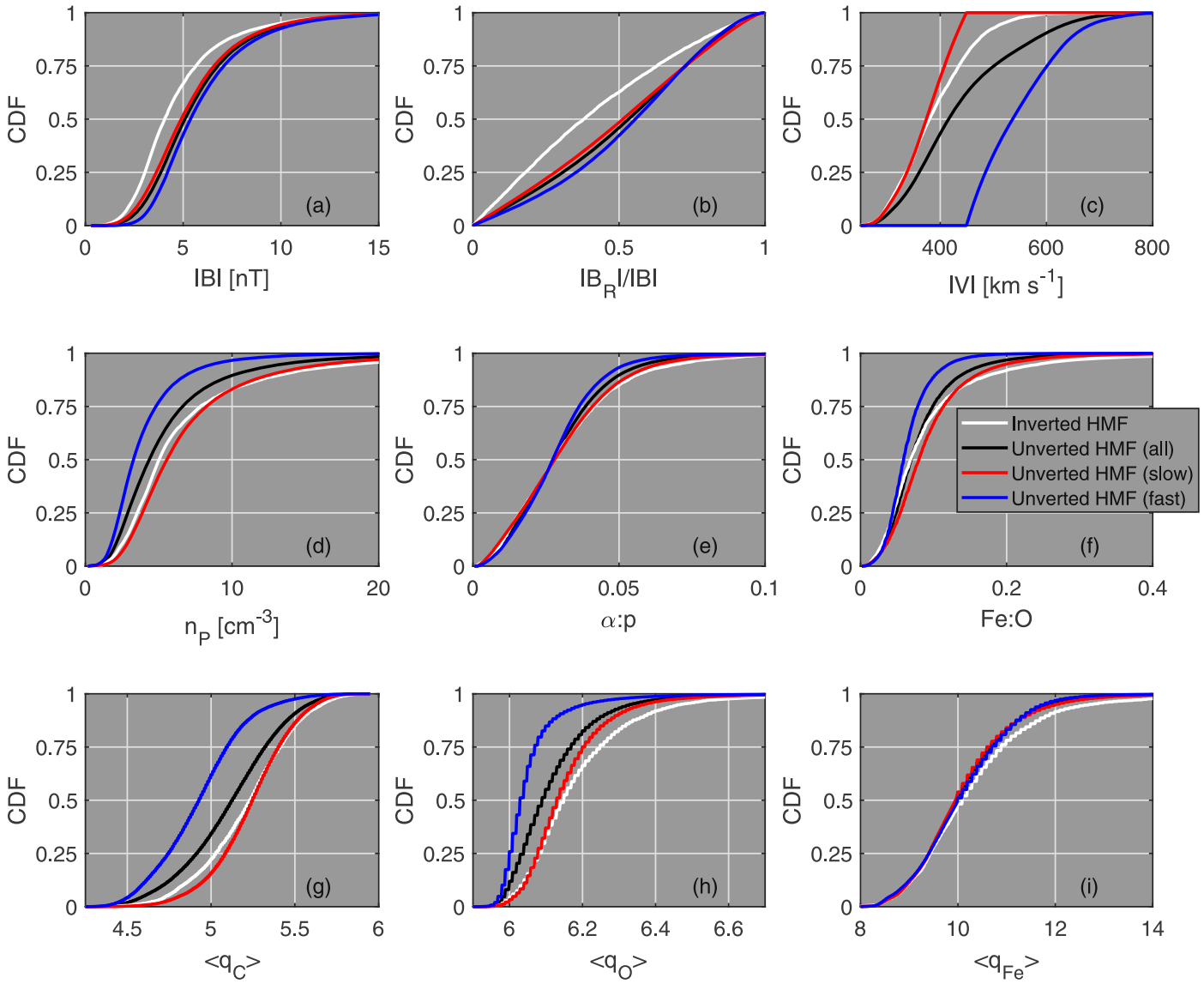

Figure 2. Cumulative distribution functions of solar wind properties of inverted (white) and uninverted (black) HMF intervals. ICMEs have been removed. Fast (blue) and slow (red) intervals of uninverted HMF are also shown. Parameters are defined in Table 1.

4. Discussion and Conclusions

Inverted HMF occurs in short bursts and preferentially in slow, dense solar wind. It generally exhibits lower HMF intensity and increased inclination to the radial direction compared to the solar wind as a whole. We have further shown that inverted HMF is similar to slow solar wind in terms of elemental composition and oxygen, carbon, and iron ion charge states, suggesting common coronal source conditions.

Inverted HMF is strongly differentiated from fast uninverted HMF in all parameters except the elemental composition measures and iron ion charge-states. Specifically, inverted HMF is weakly differentiated from fast uninverted HMF in terms of Fe:O abundance ratios, but there is little difference in the α:p abundance ratio, as is often the case with the slow wind in general (Fu et al. 2017). It is possible that gradients in elemental abundance are produced in the corona, but that differential streaming of heavy ions relative to the bulk (proton) solar wind (Berger et al. 2011; Alterman et al. 2018) is able to traverse the short inverted HMF intervals and remove this signature by 1 au (though this should equally wash out the carbon and oxygen charge-state signatures). It may be possible to identify any such compositional signatures using observations from close to the Sun, discussed below, or focusing only on the longer-lived HMF inversions, though this prohibits statistical analysis.

Interpretation of ion charge states in terms of coronal temperature is not straightforward, with coronal electron density, temperature, and plasma velocities all contributing to the observed in situ values (Zhao et al. 2014). But in general, elevated oxygen and carbon charge states are produced by increased temperatures in the lower corona, whereas elevated iron charge states are more likely to result from heating through the extended corona (Song et al. 2016). Thus inverted HMF is associated with increased heating in the lower corona, which suggests that the material was released from hot coronal loops. This is consistent with previous results that show an association between inverted HMF and closed coronal loops in dipolar and unipolar coronal streamers (Owens et al. 2013). Hot coronal material on closed coronal loops can be released by interchange reconnection (Crooker & Owens 2011) with an open magnetic

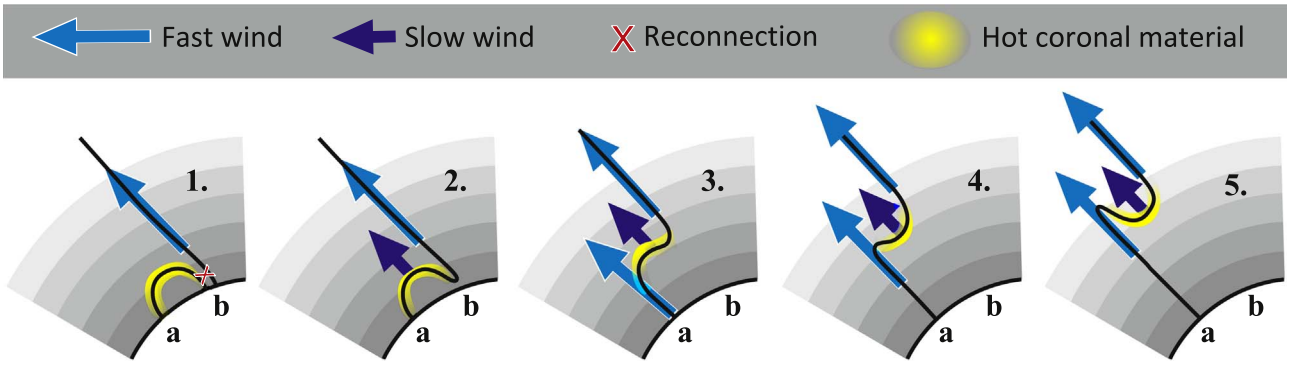

Figure 3. Schematic of inverted HMF formation. Gray shaded bands show increasing altitude through the corona. At time 1, a closed loop containing hot material (yellow shading) reconnects at point *b* with an open field line containing fast wind (light blue arrow). At time 2, inverted HMF is produced as a result of the reconnection above point b. The hot coronal material begins to rise as newly released slow solar wind (dark blue arrow). At time 3, magnetic curvature forces and solar wind shear combine to remove the HMF inversion above point *b*. Eventually, the newly open field at point *a* becomes a source of fast wind. At time 4, the resulting solar wind shear produces new inverted HMF above point *a*. At time 5, the new inverted HMF grows with increasing altitude.

Table 1
Differences between Inverted HMF and Different Populations of Uninverted HMF, for a Range of Solar wind Parameters, as Measured by β'

Solar Wind Parameter	β' for all Uninverted HMF	β' for Slow Uninverted HMF	β' for Fast Uninverted HMF
$\lvert B\rvert$[a]	−0.52	−0.44	−0.68
$\lvert B_R\rvert/\lvert B\rvert$[b]	−0.50	−0.42	−0.60
$\lvert V\rvert$[c]	−0.42	*0.1*	**−2.00**
n_P[d]	*0.24*	*−0.18*	0.70
α:p[e]	*0.02*	*−0.00*	*0.02*
Fe:O[f]	*−0.02*	−0.26	0.28
$\langle q_C\rangle$[g]	0.36	*−0.08*	**1.16**
$\langle q_O\rangle$[h]	0.54	*0.20*	**1.30**
$\langle q_{Fe}\rangle$[i]	*0.12*	*0.14*	*0.1*

Notes. Larger β' values indicate greater differences between the distributions. Absolute values above 1 are shown in bold, below 0.25 are shown in italics.
[a] Properties are magnetic field intensity.
[b] Fraction of the HMF in the radial direction.
[c] Solar wind speed.
[d] Proton density.
[e] Alpha-to-proton number ratio.
[f] Iron-to-oxygen ion number ratio
[g] Average carbon ion charge state.
[h] Average oxygen ion charge state.
[i] Average iron ion charge state.

flux tube. This could be initiated by either random foot-point motions or more large-scale convection of open flux (Fisk 2003). The inverted HMF observed at 1 au, however, is unlikely to be formed as a direct result of this reconnection, as shown schematically by Figure 3. We assume that the pre-existing open flux tube is associated with a coronal hole and thus contains low ion charge states and fast solar wind, while the newly opened coronal loop produces enhanced ion charge states and slow solar wind. The inverted magnetic flux that is initially produced by interchange reconnection at point *b* will be eroded by both the magnetic curvature forces that act to straighten magnetic flux tubes, and by the solar wind speed shear across the inversion. Given the high Alfvén speeds in the low corona and the fact that the solar wind speed shear will exist from the moment reconnection occurs, this magnetic field inversion is unlikely to survive to the upper corona and become a HMF inversion. If the inversion does survive to become part of the solar wind, it would continue to be eroded during transit to 1 au. This runs contrary to the inferred trends in HMF inversions, which suggest a growth with heliocentric distance (Owens et al. 2008), producing an excess flux in the heliosphere (Lockwood et al. 2009; though this is also the result of the increasing angle of the Parker spiral with heliocentric distance, which means "ortho-gardenhose" magnetic flux has an increasingly large radial magnetic field contribution).

Instead, we suggest that the observed inverted HMF is produced on the non-reconnecting leg of the coronal loop. At some time, *t*, after the reconnection has occurred, this newly opened flux tube will become a source of fast solar wind, particularly if the foot-point of the newly open flux tube convects deeper within a pre-existing corona hole (Fisk 2003). This creates a pattern of fast–slow–fast wind along a given flux tube and a second region of solar wind speed shear over point *a*, this time in a sense to generate inverted magnetic flux, as long as it can overcome the opposing magnetic curvature forces. If the slow/fast winds are not radially aligned, the solar wind speed shear will persist with increasing altitude in the corona, while the Alfvén speed will fall off rapidly with height due to declining magnetic field strength. Thus the inverted HMF will grow with increasing radial distance from the Sun, as long as the speed shear persists. The lifetime of the speed shear will depend on size-scale of slow/fast solar wind bursts associated with this process. Once solar wind speed shear has dissipated, the inverted HMF will be eroded at the local Alfvén speed (which itself decreases with heliocentric distance).

The degree of inversion in the HMF at a given radial distance will depend on height profile of the Alfvén speed, which can be estimated using a coronal magnetic field model and assumed plasma density profile, the magnitude of the speed sheer and the time for which the sheer has been acting, *t*. By measuring solar wind speed shear and the strength and occurrence of inverted HMF with radial distance from the Sun, *Parker Solar Probe* and *Solar Orbiter* will enable quantification of *t*, which determines how long newly opened coronal loops act as a source of slow solar wind and how quickly they transition to become sources of fast wind. This will provide an observational test of the models of slow solar wind generation by continual interchange reconnection at the

open/closed magnetic flux boundary (Fisk 2003; Antiochos et al. 2011; Crooker et al. 2012).

Work was part-funded by Science and Technology Facilities Council (STFC) grant No. ST/M000885/1 and ST/R000921/1, and Natural Environment Research Council (NERC) grant No. NE/P016928/1. Solar wind composition and ion charge-state information are provided by the *ACE* SWICS instrument, here taken from the 1 hr "merged" data set at ftp://cdaweb.gsfc.nasa.gov/pub/data/ace/multi. *ACE* solar wind magnetic field, plasma, and suprathermal electron data were obtained from ftp://cdaweb.gsfc.nasa.gov.

ORCID iDs

Mathew J. Owens https://orcid.org/0000-0003-2061-2453
Mike Lockwood https://orcid.org/0000-0002-7397-2172
Luke A. Barnard https://orcid.org/0000-0001-9876-4612

References

Alterman, B. L., Kasper, J. C., Stevens, M. L., & Koval, A. 2018, ApJ, 864, 112
Antiochos, S. K., DeVore, C. R., Karpen, J. T., & Mikić, Z. 2007, ApJ, 671, 936
Antiochos, S. K., Mikić, Z., Titov, V. S., Lionello, R., & Linker, J. A. 2011, ApJ, 731, 112
Berger, L., Wimmer-Schweingruber, R. F., & Gloeckler, G. 2011, PhRvL, 106, 151103
Cane, H. V., & Richardson, I. G. 2003, JGRA, 108, 1156
Crooker, N. U., Antiochos, S. K., Zhao, X., & Neugebauer, M. 2012, JGRA, 117, 4104
Crooker, N. U., Kahler, S. W., Larson, D. E., & Lin, R. P. 2004, JGRA, 109, A03108
Crooker, N. U., & Owens, M. J. 2011, SSRv, 172, 201
Fisk, L. A. 2003, JGRA, 108, 1157
Fu, H., Madjarska, M. S., Xia, L., et al. 2017, ApJ, 836, 169
Gloeckler, G., Cain, J., Ipavich, F. M., et al. 1998, The Advanced Composition Explorer Mission (Berlin: Springer)
Linker, J. A., Caplan, R. M., Downs, C., et al. 2017, ApJ, 848, 70
Lockwood, M. 2013, LRSP, 10, 4
Lockwood, M., Owens, M. J., & Rouillard, a. P. 2009, JGRA, 114, A11104
McComas, D. J., Bame, S. J., Barker, S. J., et al. 1998, SSRv, 86, 563
Owens, M. J., Arge, C. N., Crooker, N. U., Schwadron, N. a., & Horbury, T. S. 2008, JGR, 113, A12103
Owens, M. J., Crooker, N. U., & Lockwood, M. 2013, JGRA, 118, 1868
Owens, M. J., & Forsyth, R. J. 2013, LRSP, 10, 5
Owens, M. J., Lockwood, M., Riley, P., & Linker, J. 2017, JGRA, 112, 10980
Smith, C. W., L'Heureux, J., Ness, N. F., et al. 1998, SSRv, 86, 613
Song, H. Q., Zhong, Z., Chen, Y., et al. 2016, ApJS, 224, 27
Wang, Y.-M., & Sheeley, N. R. 1995, ApJL, 447, L143
Zhang, X. D. 2010, Stat. Biopharm. Res., 2, 292
Zhao, L., Landi, E., Zurbuchen, T. H., Fisk, L. A., & Lepri, S. T. 2014, ApJ, 793, 44